AD-A182 113 HYDROGEN CARS (COHERENT ANTISTOKES RAMAN SPECTROSCOPY) SPECTRA FROM CH(4)..(U) ARMY ARMAMENT RESEARCH DEVELOPMENT AND ENGINEERING CENTER DOV.. L E HARRIS 1/1

UNCLASSIFIED MAY 87 ARAED-TR-87014 F/G 20/5 NL

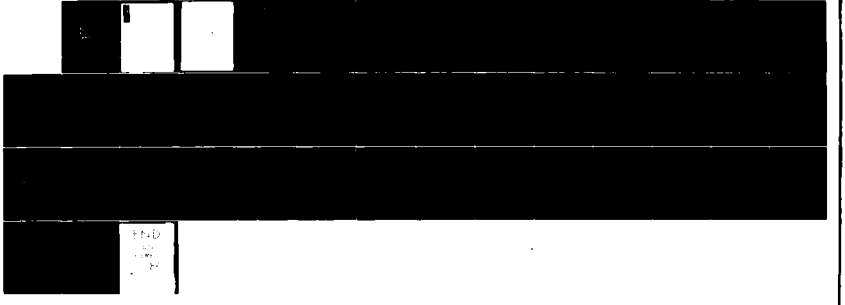

END

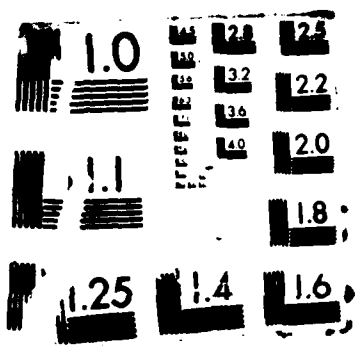
1.0
1.1
1.25
1.4
1.6
1.8
2.0
2.2
2.5
2.8
3.2
3.6
4.0

UNCLASSIFIED

SECURITY CLASSIFICATION OF THIS PAGE (When Data Entered)

REPORT DOCUMENTATION PAGE		READ INSTRUCTIONS BEFORE COMPLETING FORM
1. REPORT NUMBER Technical Report ARAED-TR-87014	2. GOVT ACCESSION NO. ADA182113	3. RECIPIENT'S CATALOG NUMBER
4. TITLE (and Subtitle) Hydrogen CARS Spectra from CH(4)/N(2)O and Nitramine Composite Flames		5. TYPE OF REPORT & PERIOD COVERED 6. PERFORMING ORG. REPORT NUMBER
7. AUTHOR(s) L. E. Harris		8. CONTRACT OR GRANT NUMBER(s)
9. PERFORMING ORGANIZATION NAME AND ADDRESS ARDEC, AED Energetics and Warheads Div (SMCAR-AEE) Picatinny Arsenal, NJ 07806-5000		10. PROGRAM ELEMENT, PROJECT, TASK AREA & WORK UNIT NUMBERS
11. CONTROLLING OFFICE NAME AND ADDRESS ARDEC, IMD STINFO Div (SMCAR-MSI) Picatinny Arsenal, NJ 07806-5000		12. REPORT DATE May 1987 13. NUMBER OF PAGES 45
14. MONITORING AGENCY NAME & ADDRESS(if different from Controlling Office)		15. SECURITY CLASS. (of this report) UNCLASSIFIED 15a. DECLASSIFICATION/DOWNGRADING SCHEDULE

16. DISTRIBUTION STATEMENT (of this Report)

Approved for public release; distribution unlimited.

17. DISTRIBUTION STATEMENT (of the abstract entered in Block 20, if different from Report)

18. SUPPLEMENTARY NOTES

This report was presented at the Flash Photolysis and Its Applications meeting in honor of Sir George Porter, PRS, at the Royal Insitition, London, 1986 and published in Journal of Chemical Society, Faraday Trans. 2, 82, 2129-2141 (1986).

19. KEY WORDS (Continue on reverse side if necessary and identify by block number)

Propellants,
Lova,
Hydrogen,
Coherent Antistokes, Raman Spectroscopy, (~~CARS~~)
Insensitive Propellant

20. ABSTRACT (Continue on reverse side if necessary and identify by block number)

The hydrogen spectra from the CH(4)/N(2)O and nitramine composite flames allow use of each of the concurrent capabilities of CARS: (1) rovibrational state resolution better than a wavenumber, (2) time resolution better than 10 nrs, and (3) spatial resolution better than 100 micrometers. The rovibrational state resolution results in direct observation of previously unobserved higher J transitions in the Q branch v" = 0 and v" = 1 and S branch v" = 0 transitions. These transitions are in accord with transitions calculated from ab initio resluts and with transitions indirectly obtained from electronic emission ~~(cont)~~ cont'd

DD FORM 1 JAN 73 1473 EDITION OF 1 NOV 65 IS OBSOLETE

UNCLASSIFIED

SECURITY CLASSIFICATION OF THIS PAGE (When Data Entered)

20. Abstract: (cont)

cont'd

spectra. The ab initio results give a compact set of constants that gives results within the experimental accuracy of the CARS experimental results.

The experimental transition energies were used to construct Boltzmann plots that allow discrimination among the various spectra used to determine temperature.

CARS provides the spectral resolution and intensity to allow direct observation of previously unobserved hydrogen higher J and v rotational transitions. These transitions were used to obtain temperature profiles and in the CH(4)/N(2) and nitramine composite flames that require both the high spatial and temporal resolution of CARS. These temperature profiles provided additional confirmation of previous kinetic mechanisms used to explain observations in the nitramine composite flame. The concurrent capabilities of CARS used here demonstrate its high potential for use as the probe beam in kinetic flash photolysis and direct in situ measurements of combustion flames.

Keywords:

CONTENTS

TABLES

FIGURES

INTRODUCTION

Coherent Antistokes Raman Spectroscopy (CARS) provides one of the most powerful new techniques for monitoring the progress of fast chemical reactions in uses such as the probe beam in flash photolysis. Electronic spectroscopy was first used as the probe beam in flash photolysis as originally developed by Norrish and Porter (ref 1). Similarly to electronic spectroscopy, CARS has also been extensively used for analysis of flames (refs 2 through 4) prior to use as the probe beam in flash photolysis, as for example, in refs 5 and 6. CARS allows direct monitoring of the rovibrational state distributions of reactant, transient, and product species. In addition, the nonlinear scattering processes from which CARS originates enables excellent time resolution, presently shorter than 10 ns (ref 4). CARS can also be easily optically configured to give a sampling extent less than 100 μm. These concurrent capabilities, rovibrational state resolution better than a wavenumber, time resolution better than 10 ns, and spatial resolution better than 100 μm, allow direct observation of the fast combustion reactions occuring in the reaction zone of flames where preceptible chemical change was spatially resolved on the scale of the sampling extent. This was first demonstrated experimentally in studies of the reaction zone of lean CH_4/N_2O flames (refs 2 and 3) where decay of N_2O and concomitant N_2 formation were simultaneously observed on a 100 μm spatial scale (which corresponds to millisecond time resolution for the burning velocity of the flame studied).

This capability was subsequently extended to the reaction zone of rich CH_4/N_2O flames and the flames of solids (the nitramine RDX, hexahydro-1,3,5,-trinitro-3-triazine in an organic ester matrix) (refs 7 through 9).

Spectra were obtained in the regions 4200-3900, 2400-2050, and 1900-1200 cm^{-1}. The reaction zone of the rich CH_4/N_2O flame was studied primarily to provide a stationary flame analog to the transient propellant flame. In the CH_4/N_2O flames, the decay of the initial products was observed through the Q branch of the ν_1 and ν_3 modes of N_2O and Q, O, and S branches of the ν_2 and $2\nu_2$ modes of CH_4. The formation of the products N_2, H_2[Q(v" = 0 and v" = 1) and S(5) - S(9)], CO, and CO_2 (ν_1) were also observed. In the nitramine propellant flame near the surface of the propellant, reactant RDX (1599 cm^{-1} tentatively assigned as asymmetric NO_2 stretch) and transients HCN (ν_1) and NO are observed at moderate concentration (>1%). The final product N_2 is observed at low concentration (~ 1%); H_2 (Q and S branches) and CO are observed at higher concentration ($\geq$10%). RDX and HCN decay within 2 mm of the propellant surface, while NO remains constant until 4 mm, where it decays with a concomitant rise in N_2 concentration and temperature. H_2 and CO also increase in temperature and concentration. The nitramine reaction zone was seen to consist of two regions characterized by the reactions of RDX and HCN near the surface, consistent with the high-temperature mechanism of RDX decomposition, and the conversion of NO to N_2 to generate the luminous flame further above the surface.

The observed spectra demonstrate many of the features previously discussed which make CARS useful for the probe beam in flash photolysis. This is clearly

seen in the rotationally well-resolved hydrogen spectra from the reaction zone of rich CH_4/N_2O and nitramine composite flames. These CARS hydrogen spectra are treated here in greater detail than that given in previous reports (refs 7 through 9). Higher rotational transitions in the Q and S branches of the ground and first excited vibrational state, many of which were directly observed for the first time (ref 10), are compared to transitions calculated from constants derived from ab initio calculations (ref 11) and transitions calculated from those observed in the rovibrational structure of electronic emission spectra (ref 12). These hydrogen transitions are used to obtain temperature profiles through the reaction zone of rich CH_4/N_2O flames and, for the first time, of nitramine composite flames. The interpretatins involved in the reduction of the hydrogen data remove some of the ambiguities of data interpretation previously reported (ref 9). These observed temperature profiles aid in the interpretation of the observed species in terms of elementary reactions.

Flash photolysis using CARS as the probe beam will be used in future work for determining the elementary reactions required to elucidate the kinetic mechanisms directly observed using CARS. Consequently, CARS will be useful not only for observing combustion flame phenomena directly in situ but also using the same or similar apparatus for elucidating these phenomena through elementary reactions determined using flash photolysis and related techniques.

EXPERIMENTAL

CARS spectra were generated using the folded BOXCARS apparatus (ref 9). Briefly, the output of the Quantra-Ray DCR-2A Nd/YAG laser at 1.06 μm (700 mJ) is doubled to generate the pump beam at 5320A (250 mJ) with a bandwidth of near 1 cm^{-1}. The pump beam is split to generate ω_{1s} and ω_{1p}. ω_{1s} is used to pump a dye laser to generate the Stokes beam ω_2. The dye laser consists of a flowing dye cell in a planar Fabry-Perot oscillator cavity pumped slightly off-axis by 20% of ω_{1s}, with the output amplified by an additional flowing dye cell pumped by the remainder of ω_{1s}. The dye laser is operated broadband with the laser dyes Exciton DCM and LDS in ethanol to generate a nonresonant spectra centered near 4210 cm^{-1} with a bandwidth of 300 cm^{-1} for H_2 v = 0 Q branch spectra. ω_1 is split such that ω_1, ω_1', and ω_2 are placed on a 12.5 mm circle. ω_3 was focused into a monochromator equipped with a PAR SIT detector interfaced to a PAR OMA2 system. The full-width-at-half-maximum (FWHM) of calibration lines near the center of the SIT detector is 3.0 cm^{-1}, giving approximately 1 cm^{-1} per channel over the spectral range investigated.

Stationary flame measurements were made on a premixed CH_4/N_2O flame maintained on a circular burner with a 2.0-cm-diameter head whose surface was constructed of a matrix of steel syringe needles of 1 mm outer diameter. A mixture of Matheson technical grade methane and chemically pure nitrous oxide were flowed through the burner at 13 cm/s to maintain a 3.2 equivalence ratio (ϕ)

flame, where ϕ is defined as the fuel/oxidant ratio divided by the stoichiometric fuel/oxidant ratio. To obtain CARS spectra in the reaction zone, the center of the burner surface was displaced vertically at intervals of 0.5 mm (0.25 mm in the vicinity of the reaction zone). The nitramine composite grains burned were 14 x 14 mm^2 cylinders of mass 3.2 g. The composite consisted of 76% RDX (hexahydro-1,3,5,-trinitro-s-triazine), 20% carbohydrates, and 4% nitrocellulose. The propellant grains were burned in air with spectra taken along the centerline above the burning propellant surface during the approximately 1-min burn time. The calculated approximate gas velocity from the burning cylinder is 50 cm/s. Thermochemical calculations were performed for both the CH_4/N_2O flame and nitramine composite flames. The calculated flame temperature for CH_4/N_2O was 1745 K with 23% CO, 1% CO_2, 42% H_2, 5% H_2O, and 29% N_2; and for the nitramine composite 2076 K with 27% H_2, 22% N_2, 10% H_2O, 3% CO_2, and 38% CO.

RESULTS

The observed CARS spectrum in the isolated line approximation (ref 13) is proportional to the square of the modulus of the third-order susceptibility ($\chi^{(3)}$) which is the sum of a resonant term χ_r related to nuclear displacement and χ_{nr} related to electronic displacement. χ_r is composed of a real component χ', which displays dispersive behavior and an imaginary component χ which displays resonant behavior such that:

$$\left|\chi^{(3)}\right|^2 = \left|\chi' + \chi'' + \chi_{nr}\right|^2 = \sum_j \left|\frac{kj\,\Gamma j}{2\,\Delta\omega j - i\Gamma_j} + \chi_{nr}\right|^2 \qquad (1)$$

$$kj = (N/M\omega o)\left|M_j\right|^2 (\Delta j)\,\Gamma_j^{-1} \qquad (2)$$

where M_j, Δj, and Γj are the polarizability matrix element, normalized population difference and line width, respectively, $\Delta\omega_j = \omega_1 - \omega_2 - \omega_j$, m is the reduced mass, ω_o is the resonant Raman frequency, and N is the molecular gas density. $M = \alpha^2(\nu + 1)$ and $7/45\ bj\ \nu^2\ (\nu + 1)$ for Q and O, S branches, respectively, where α, ν, and b_J are the derivatives of the mean isotropic and anisotropic molecular polarizability, and b_J are the Placzck-Teller coefficients, ν is the vibrational quantum number, and $(\nu + 1)$ is contributed by the vibrational matrix element.

The interpretation of hydrogen CARS spectra under the conditions in which it is observed here is particularly straightforward. The Raman cross section of hydrogen (from which Mj can be calculated) is sufficiently large (it is twice that of nitrogen) that at the hydrogen concentrations observed in most of these experiments, the effect of the χ_{nr} may be neglected. In this case, the peak CARS intensity, Ij^{max}, is given by the imaginary component of $\chi^{(3)}$

$$(Ij^{max})^{1/2} = \frac{(N \quad)}{m\omega_o} \left| Mj \right|^2 (\Delta j)\, \Gamma j^{-1}$$

Neglecting the aniostropic component of Mj and defining $\Delta j = (2J + 1)\, gj\, \bar{\Delta} j$ where gj is the nuclear spin statistical degeneracy (g = 3 for odd levels and g = 1 for even levels) and $\bar{\Delta} j$ is the population difference per rotational energy level

$$(\bar{Ij}^{max})^{1/2} = \frac{(Ij^{max})^{1/2}}{(2J + 1)\, g_j\, (\nu + 1)} = (\frac{N}{m\, \omega_o}) \alpha \left| {}^2 \Gamma_j^{-1} \bar{\Delta} j \right.$$

Γj^{-1} as observed in these experiments is determined by the convolution of the instrument response function (FWFM = 3.0 cm^{-1}) over the doppler broadened transitions (where the linewidth is of the order of tenths of a wavenumber). Under these conditions the observed linewidth is effectively constant and equal to that of the instrument. Therefore, $(Ij^{max})^{1/2}$ is related by a constant to $\bar{\Delta} j$. If the excited state population is neglected, $\bar{\Delta} j$ can be assumed to be given by the Boltzmann relation $\bar{\Delta} j = \exp\left[\frac{-k\, \Delta Ej}{T}\right]$

The relation

$$\ln (\bar{Ij}^{max}) = C \frac{k}{T} \Delta Ej$$

(where k is the Boltzmann constant) can be used to determine temperature from the peak heights. The separation of the rotational lines and the lack of modulation by χ_{nr} eliminate the complexities of data reduction recently considered (ref 13).

CH_4/N_2O Flames

A summary of the species observed for the ϕ = 3.2 rich CH_4/N_2O flame is given in table 1. Hydrogen Q-band structure as it increases through the reaction zone is shown in figure 1. Hydrogen is seen at a concentration less than 1% at 4 mm. The line positions as shown for v" = 0 (fig. 1) and v" = 0, $J \leq 11$ and v" = 1, $J \leq 9$ (fig. 2), and the S bands J = 5 - 9 (table 1) for v" = 0 are compared to experimentally determined transitions (ref 12) and to transitions calculated from spectroscopic constants derived from ab initio calculations (ref 11). The constants given in table 2 are the same as those given in ref 11 with the exception that typographical errors for H_1 and H_2 have been corrected. These constants (table 2) result in transition energies (tables 3 and 4) that agree with rovibrational transition energies obtained from analysis of the Lyman $B^1 \Sigma_u^+ \rightarrow X^1 \Sigma_g^+$ and Werner $C^1 \Pi_u \rightarrow X^1 \Sigma_g^+$ electronic transitions. The directly observed rovibrational transitions agree within their 1 cm^{-1} experimental accuracy with both the previously observed experimental and calculated transitions. The advantage of the constants given in table 2 is that they agree with the CARS data within the experimental error and are in a compact form convenient for use in spectral analysis.

Higher than 8 mm above the burner surface there is an apparent bimodal distribution in which approximately half of the observed spectra have Boltzmann distributions consistent with the random experimental error, while the other spectra show deviations from a Boltzmann distribution which is much larger (greater then 2σ). An example of this behavior is illustrated by Boltzmann plots shown in figures 3 and 4. At the same position in the flame (18 mm above the burner surface) spectra taken under similar conditions give widely disparate temperatures. However, of the two distributions only the lower temperature result appears Boltzmann. In the non-Boltzmann distributions, the odd levels are preferentially populated over the even levels. While these apparently non-Boltzmann distributions may reflect the actual hydrogen rotational distribution, it seems more likely due to flame instability which increases with distance above the burner. The outer blue diffusion flame is noticeably floppy and of higher temperature than the adiabatic CH_4/N_2O flame. Spectra which result from a mixture of adiabatic and diffusion flames due to flame flicker would yield non-Boltzmann results perhaps similar to that in figure 4. Use of only Boltzmann results allows construction of the temperature profile shown in figure 5.

Nitramine Composite Flames

A summary of species observed in the nitramine composite flame is given in table 5. Average spectra (100 scans, 10 s) were taken as a function of distance from the propellant surface to 6 mm above the surface at intervals of 1 mm. Each spectrum was taken nominally 10 s after ignition. In addition, time sequences of ten-scans (1 s) spectra were taken approximately every 6 s from ignition to extinction. The intensity of the H_2 signal permitted acquisition of single-shot spectra. Time-resolved spectra of the H_2 Q branch at the propellant surface are given in figures 6 and 7. Single-shot spectra (fig. 6) are obtained at good signal-to-noise and are in substantial agreement with 10-shot averaged spectra (fig. 7). The reduction of the signal-to-noise ratio from bottom to top is a reflection of the increasing temperature as a function of distance above the propellant surface. Average spectra taken 12 and 18 seconds after ignition were used to construct the temperature profile shown in figure 8. The average surface temperature is 1100 K $\pm$ 200 K (averaging data taken within 2 mm of the surface). The dispersion reflects not only the noise in the individual spectra but also the variation of the distance of the surface with respect to the CARS sampling volume, since spectra are taken as close to the surface as possible. Both sets of spectra show the same trend, i.e., an increase in temperature from the surface to 4 mm where the temperature levels off at 2000 K which is close to the calculated adiabatic flame temperature. The spread of the data is such that the functional form of the variation of temperature with distance is difficult to determine. One of the simplest interpretations is to consider all points within 2 mm of the surface as equivalent with the lowest temperature measured (900 $\pm$ 100 K) being considered as the upperbound of the gas-surface interface temperature. Alternatively, both sets of data may be taken as indicating a decrease in temperature from the surface to about 2 mm. More precise data are needed to determine the precise functional form of the temperature gradient near the surface.

DISCUSSION

The H_2 spectra from the CH_4/N_2O and nitramine composite flame allow use of each of the concurrent capabilities of CARS: (1) rovibrational state resolution better than a wavenumber, (2) time resolution better than 10 ns, and (3) spatial resolution better than 100 μm . The revibrational state resolution results in direct observation of previously unobserved higher J transitions in the Q-branch v" = 0 and v" = 1 and S-branch v" = 0 transitions. These transitions are in accord with transitions calculated from ab initio results and with transitions indirectly obtained from electronic emission spectra (tables 3 and 4). The ab initio results (ref 10) give a compact set of constants given in table 2 that give results within the experimental accuracy of the CARS experimental results.

The experimental transition energies have been used to construct Boltzmann plots (examples of which figs. 3 and 4) that allow discrimination among the various spectra used to determine temperature. A bimodal temperature distribution is obtained above a certain height from the burner surface. However, only the lower temperatures, which are in accord with the calculated flame temperature, give a Blotzmann plot consistant with the experimental error. This is perhaps indicative of the influence of flame flicker; although, the occurrence of a certain fraction of nonequilibrated ortho/para hydrogen cannot be definitively discounted. Whatever the source of the non-Boltzmann hydrogen distributions, it is clear that these cannot be used to obtain temperature, which is only defined in the context of a Blotzmann distribution.

Use of this Boltzmann discrimination allows construction of temperature profiles in both CH_4/N_2O (fig. 5) and nitramine composite flames. Reaction occurs over a region extending from 2 mm to 14 mm with the steepest concentration gradients occurring between 10 mm and 14 mm with a post flame region above 14 mm. As given in table 1, only decay of the initial products was observed through the Q branch of the ν_1 NN and ν_3 NO stretching modes of N_2O and the Q, O, and S branches of the ν_2 and $2\nu_2$ modes of CH_4. No intermediate species were detected. Initial decomposition of the reactants was observed to occur near 500 K. Secondary reactions for N_2O given by Balaklnine et. al. (ref 14)

$$H + N_2O \text{ ---> } N_2 + OH \qquad k = 6 \times 10^{13} \exp(-13100/RT)$$

and CH_4 given by Tabayaski and Bauer (ref 15)

$$CH_4 + H \text{ ---> } CH_3 + H_2 \qquad k = 7.23 \times 10^{14} \exp(-15600/RT)$$

explain the reactivity at 500 K.

The conversion of methane to final products is thought to proceed by the following global mechanism (ref 16)

$$CH_4 \text{ ---> } CH_3 \text{ ---> } CH_2O,\ CHO \text{ ---> } H_2,\ CO.$$

The conversion of fuel-bound nitrogen is an area of active current research, thought to occur by the global mechanism (refs 17 and 18)

$$\text{Fuel N} \longrightarrow \text{HCN} \longrightarrow \underset{\text{NO}}{\overset{\text{NH}_i \longrightarrow \text{NO}}{\longrightarrow}} \; \text{N}_2 \qquad i = 0, 1, 2$$

The CH_4/N_2O flame results provide a comparison for results obtained in nitramine composite flames.

The Boltzmann criteria discussed above was also used to obtain a temperature profile in the nitramine composite flame (fig. 8) as a function of time after ignition. Fewer non-Boltzmann distributions were encountered in the nitramine composite flame than in the CH_4/N_2O flame. The spectra taken at 12 and 18 seconds after ignition give similar results within the experimental error. If the data within 2 mm of the surface are averaged, a temperature of 1100 $\pm$ 200 K is obtained. The lower-bound of the averaged data is 900 $\pm$ 100 K which maybe identified with the upper-bound of the gas/surface interface temperature. However, the temperature profile may be interpreted alternately as showing a temperature decrease from the surface to 2 mm. Above 2 mm, both sets of data show a temperature increase to 4 mm where the temperature levels off near the calculated abiabatic flame temperature of 2076 K. This temperature profile is consistent with the previous observation of RDX and HCN at the surface and decaying within 2 mm of the surface, with NO remaining constant to 4 mm. Near 4 mm, NO decayed rapidly with a concomitant increase in N_2 concentration. H_2, CO, and CO_2 increased in concentration throughout this region. These observations are qualitatively consistent with the kinetic mechanism previously invoked to explain spectra obtained in the nitramine composite flame (ref 9).

The observation of HCN and RDX and lack of observation of N_2O (<0.1%) is consistent with the high temperature (T>600K) nitramine decomposition mechanism.

$$(CH_2NNO_2)_3 \longrightarrow 3HCN + 6NO_2 + 3H_2$$

(NO_2 is not observable by CARS under the condition of the experiment.) Therefore, RDX decomposition, as opposed to processes occuring in the CH_4/N_2O flame, allows a direct buildup of the intermediates HCN and NO near the propellant surface so that they are directly observable in CARS. At these pressures, it is the decomposition processes of the species at the surface, RDX and HCN, that supply the heat that determines the burning rate of the nitramine propellant. NO conversion to N_2, which provides the heat for the luminous flame occurs too far upstream to affect the surface.

The reaction zone of nitraine propellant as thus seen to consist of two characteristic areas: (1) an inner flame area near the solid gas interface, which is at a temperature above 900 $\pm$ 100 K and is characterized by the gas-phase reactions of RDX and HCN that provide the heat that determine the burning rate and (2) an outer flame area where NO is converted to N_2 to generate the luminous flame.

CARS provides the spectral resolution and intensity to allow direct observation of previously unobserved hydrogen higher J and v rotational transitions.

These transitions have been used to obtain temperature profiles in the CH_4/N_2O and nitramine composite flames which require both the high spatial and temporal resolution of CARS. These temperature profiles have provided additional confirmation of previous kinetic mechanisms used to explain observations in the nitramine composite flame. These concurrent capabilities of CARS used here demonstrate the high potential of CARS for use as the probe beam in kinetic flash photolysis and direct in situ measurements of combustion flames.

Table 1. Summary of species identified in a $\phi = 3.2$ CH_4/N_2O flame

Observed I_{max} (cm^{-1})	Species	Comment
4155-4075	H_2 Q branch	Intensity increases up the reaction zone
3240-3100	CH_4 ($2\nu_2$)	Rapid decrease in reaction zone
2325	N_2	Gradual increase in reaction zone
2222	N_2O (ν_3)	Rapid decrease in reaction zone
2136	CO	Increase in reaction zone
2129	H_2 S(9)	Rapid increase of intensity in reaction zone; large compared to CO
1813	H_2 S(7)	Intensity increases up the reaction zone
1636	H_2 S(6)	Weak signal seen in post flame
1531	CH_4 (ν_2)	Gradual decrease in reaction zone
1447	H_2 S(5)	Intensity increases up the reaction zone
1294	N_2O (ν_1)	Intense signal that decreased rapidly in reaction zone

Table 2. Hydrogen spectroscopic constants derived from ab initio calculations

W_e	4400.39	Be	60.7922
X_eW_e	120.814	α_e	-3.0320
Y_eW_e	0.7241	γ_e	0.0350
Z_eW_e	0.0	H_0	3.23×10^{-5}
D_e	0.0448	H_1	-8.00×10^{-9}
β_e	-0.0016	H_2	-5.00×10^{-8}
δ_e	4.5×10^{-5}		

$$E(v, J) = W_e (v + 0.5) - X_eW_e(v + 0.5)^2 + Y_eW_e(v + 0.5)^3 - Z_eW_e(v + 0.5)^4 + B_v J(J + 1) - D_vJ^2 (J + 1)^2 + H_v J^3(J + 1)^3$$

$$B_v = B_e + \alpha_e (v + 0.5) + \gamma_e (v + 0.5)^2$$

$$D_v = D_e + \beta_e (v + 0.5) + \delta_e (v + 0.5)^2$$

$$H_v = H_o + H_1 (v + 0.5) + H_2 (v + 0.5)^2$$

Table 3. Raman frequencies (cm^{-1}) of H_2 Q-transitions

J	Calculations	v" = 0, Q(J)*	Observed	Calculations	v" = 1, Q(J)*	Observed
0	4161.11	4161.14		3926.00	3925.79	
1	4155.20	4155.25	4154	3920.23	3920.06	3919
2	4143.4	4143.47	4143	3908.70	3908.47	3907
3	4125.79	4125.87	4126	3891.50	3891.29	3892
4	4102.48	4102.58	4102	3868.73	3868.50	3868
5	4073.61	4073.74	4073	3840.52	3840.20	3840
6	4039.37	4039.52	4038	3807.03	3806.92	3806
7	3999.96	3999.87	4000	3768.47	3768.24	3768
8	3955.64	3956.04	3954	3725.06	3724.35	3725
9	3906.69	3906.31	3905	3677.08	3676.52	3676
10	3853.42	3852.98	3853	3568.52		
11	3796.19	3795.09	3794	3508.62		

* T. Haw, W. Y. Cheung, G. C. Chiu, and L. E. Harris, "A study of Flame Species Using CARS," 40th Symposium on Molecular Spectroscopy, Ohio Stante University Abstract WH10, ; 106 (1985).

Table 4. Raman frequencies (cm^{-1}) of H_2 S-transitions

J"	Calculated for v" = 0, S(J")*		Observed
0	354.13	354.35	
1	586.74	587.04	
2	814.22	814.43	
3	1034.67	1034.67	
4	1246.37	1245.98	
5	1447.80	1447.36	1447
6	1637.69	1636.97	1636
7	1815.08	1814.40	1813
8	1979.37	1979.08	
9	2130.32	2130.06	2129

* T. Haw, W. Y. Cheung, G. C. Chiu, and L. E. Harris, "A Study of Flame Species Using CARS," 40th Symposium on Molecular Spectroscopy, Ohio State University Abstract WH10, p 106 (1985).

Table 5. Summary of species identified in nitramine propellant flame

Observed I_{max} (cm^{-1})	Species	Command
4155-4075	H_2 Q branch	Temperature calculations indicate a temperature of 900 K at the surface of the propellant
2325	N_2	Slow increase until near the end of reaction zone where a large increase occurs
2136	CO	Intensity increases up reaction zone
2129	H_2 S(9)	Similar intensity to CO observed
2086	HCN (ν_1)*	Strong signal initially which diminishes rapidly
1872	NO	Low concentration modulation which remains constant throughout reaction zone; decreases rapidly at end of reaction zone
1814	H_2 S(7)	Signal intensity increases up the reaction zone
1599	RDX (NO_2 asymetric stretch)*	Modernate concentration early in the reaction zone
1447	H_2 S(5)	Intensity increases up the reaction zone
1387	CO_2 (ν_1)	Moderate intensity early in reaction

---

* Tentative

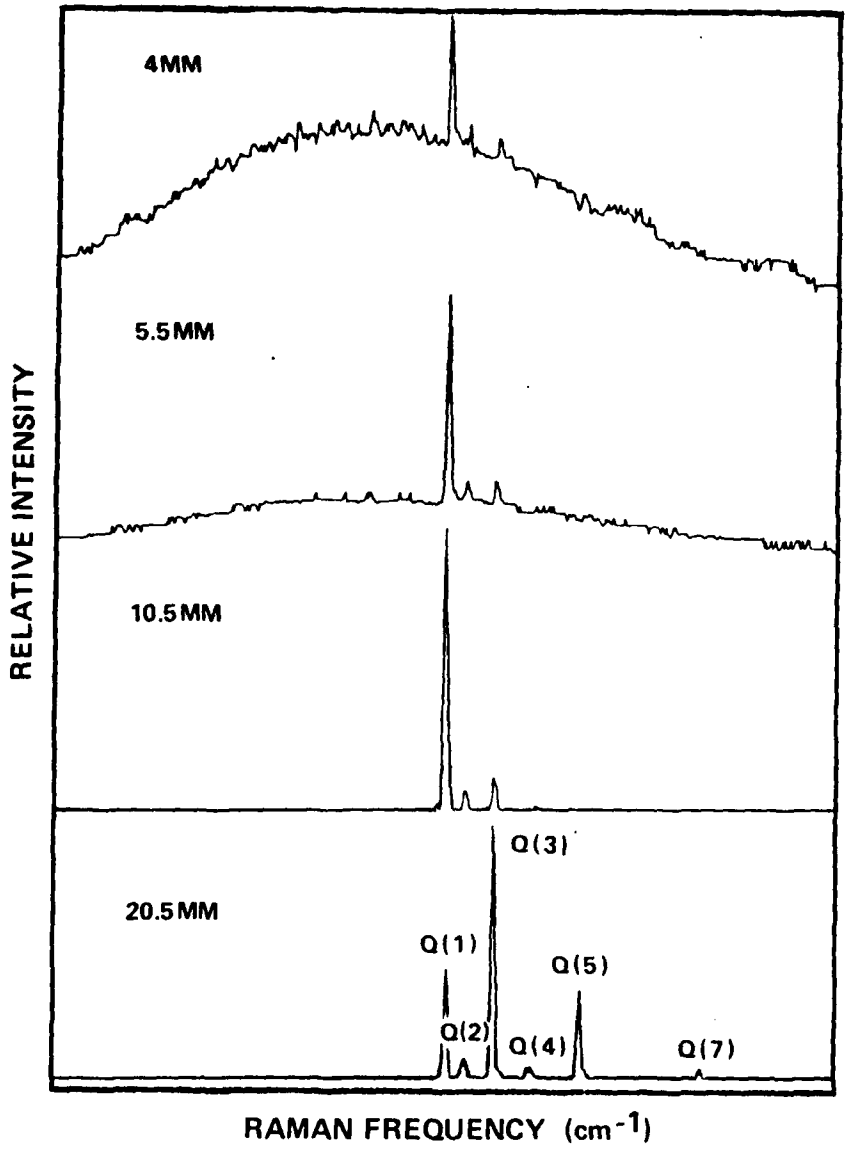

Figure 1. CARS spectra of the H_2 Q branch ($v'' = 0$) in a $\phi = 3.2$ CH_4/N_2O flame

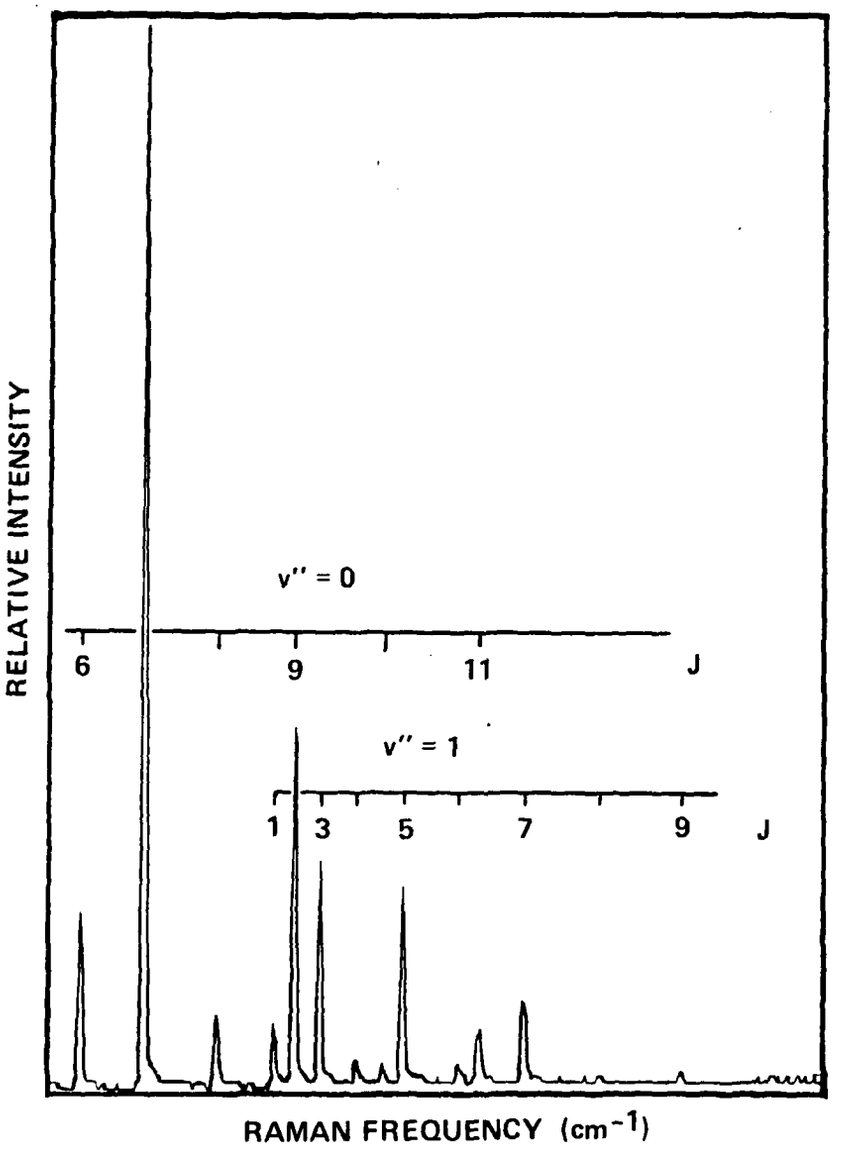

Figure 2. CARS spectra of the H_2 Q branch (v" - 0 and v" = 1) in a ϕ = 1.8 CH_4/N_2O flame

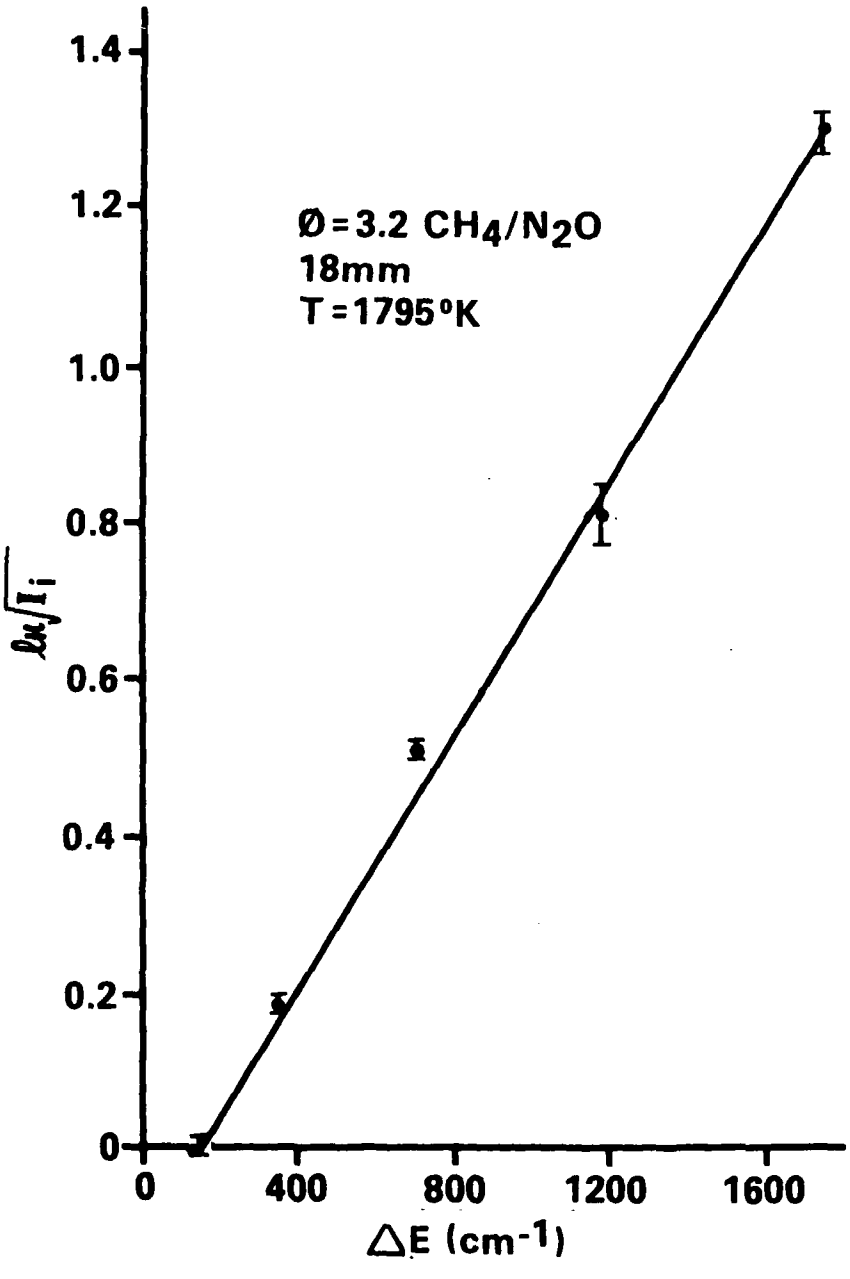

Figure 3. $\ell n \sqrt{Ii}$ versus ΔE (cm^{-1}) for a ϕ = 3.2 CH_4/N_2O flame at 18 mm above the burner surface, T = 1795K

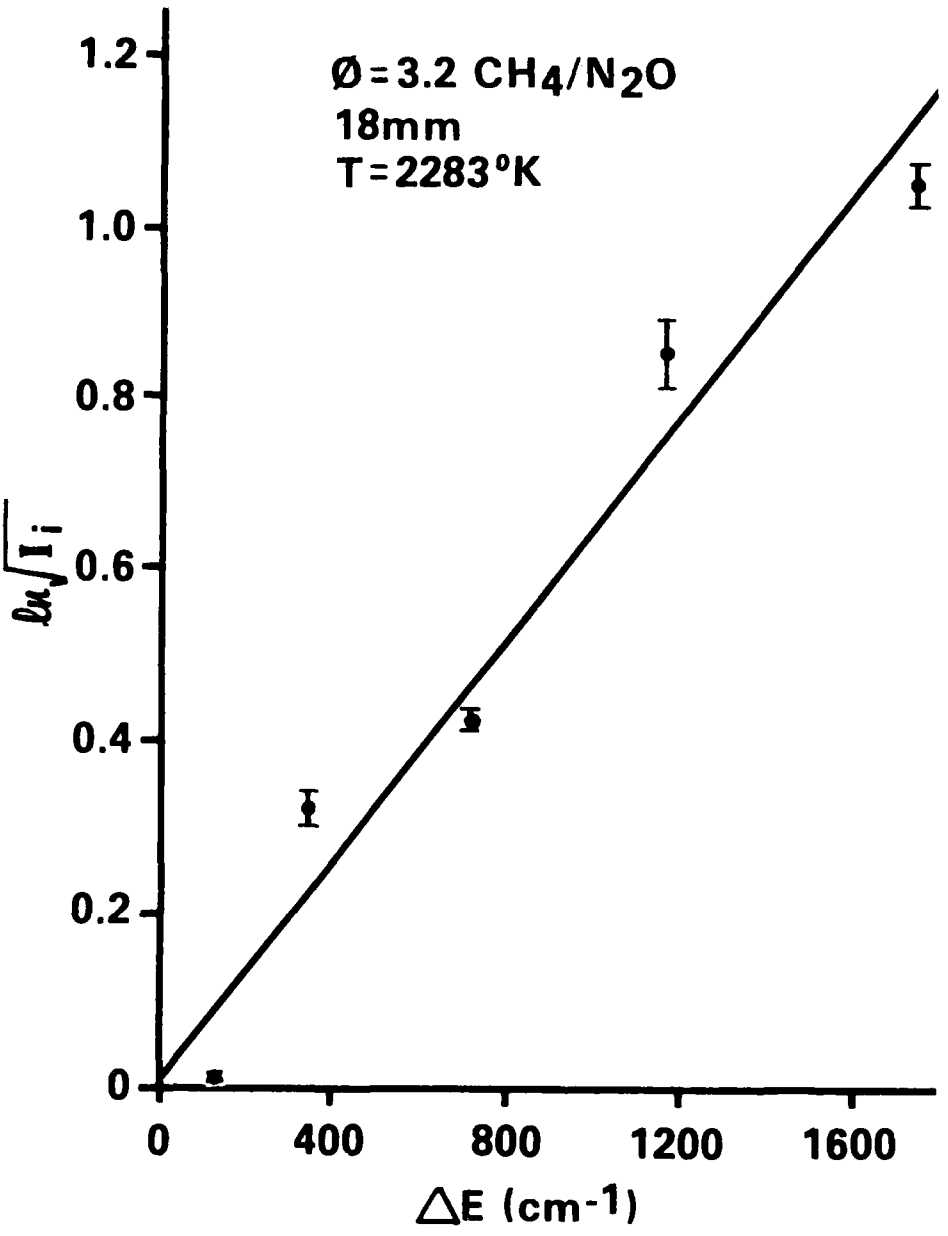

Figure 4. $\ell n \sqrt{I_i}$ versus E (cm^{-1}) for a ϕ = 3.2 CH_4/N_2O flame at 18 mm above the burner surface, T = 2283K

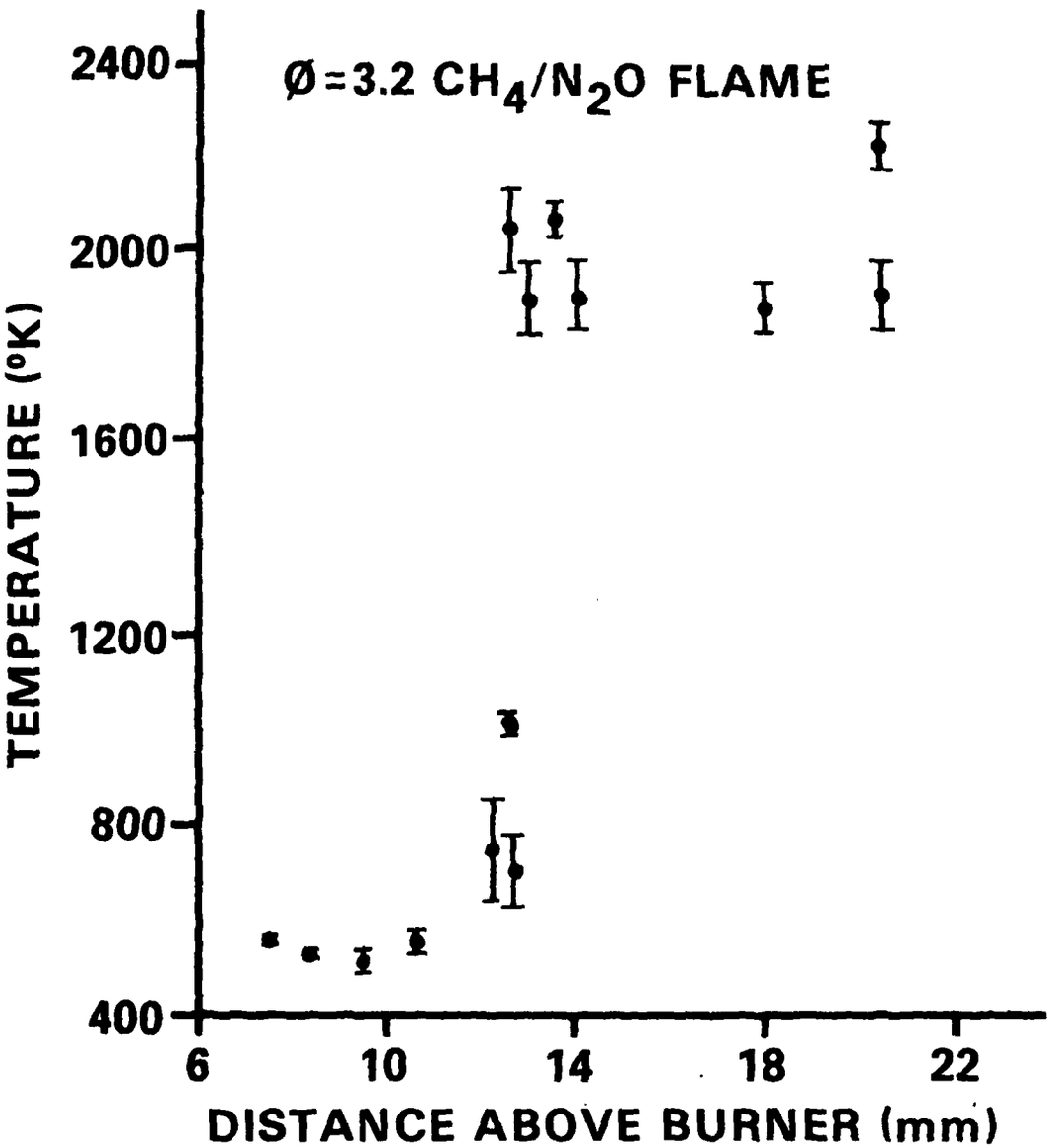

Figure 5. Temperature versus distance above burner for a $\phi = 3.2$ CH_4/N_2O flame

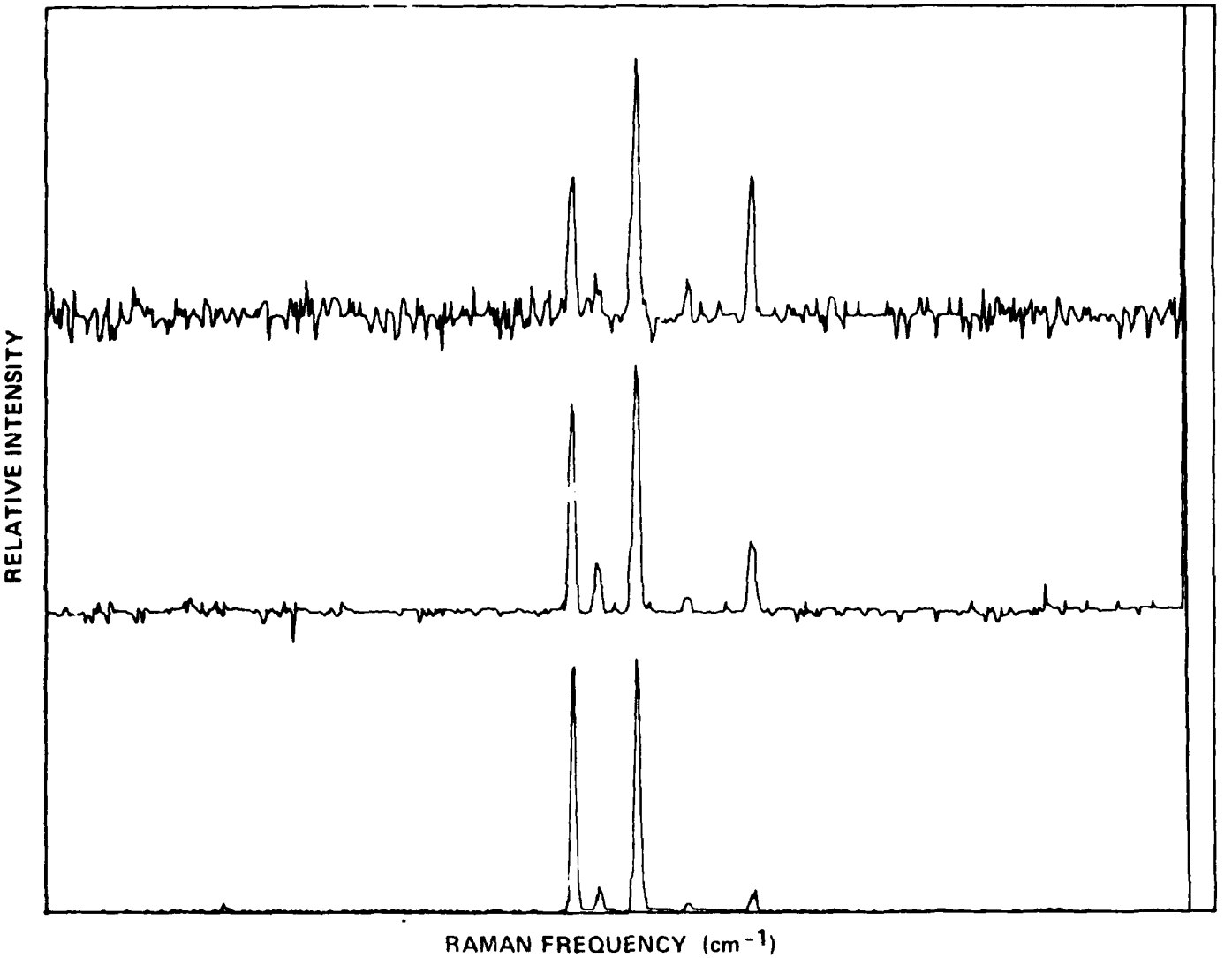

Figure 6. Time resolved (single-shot) CARS spectra of the H_2 Q branch taken at nominal 6-sec intervals after ignition and shown sequentially from bottom to top

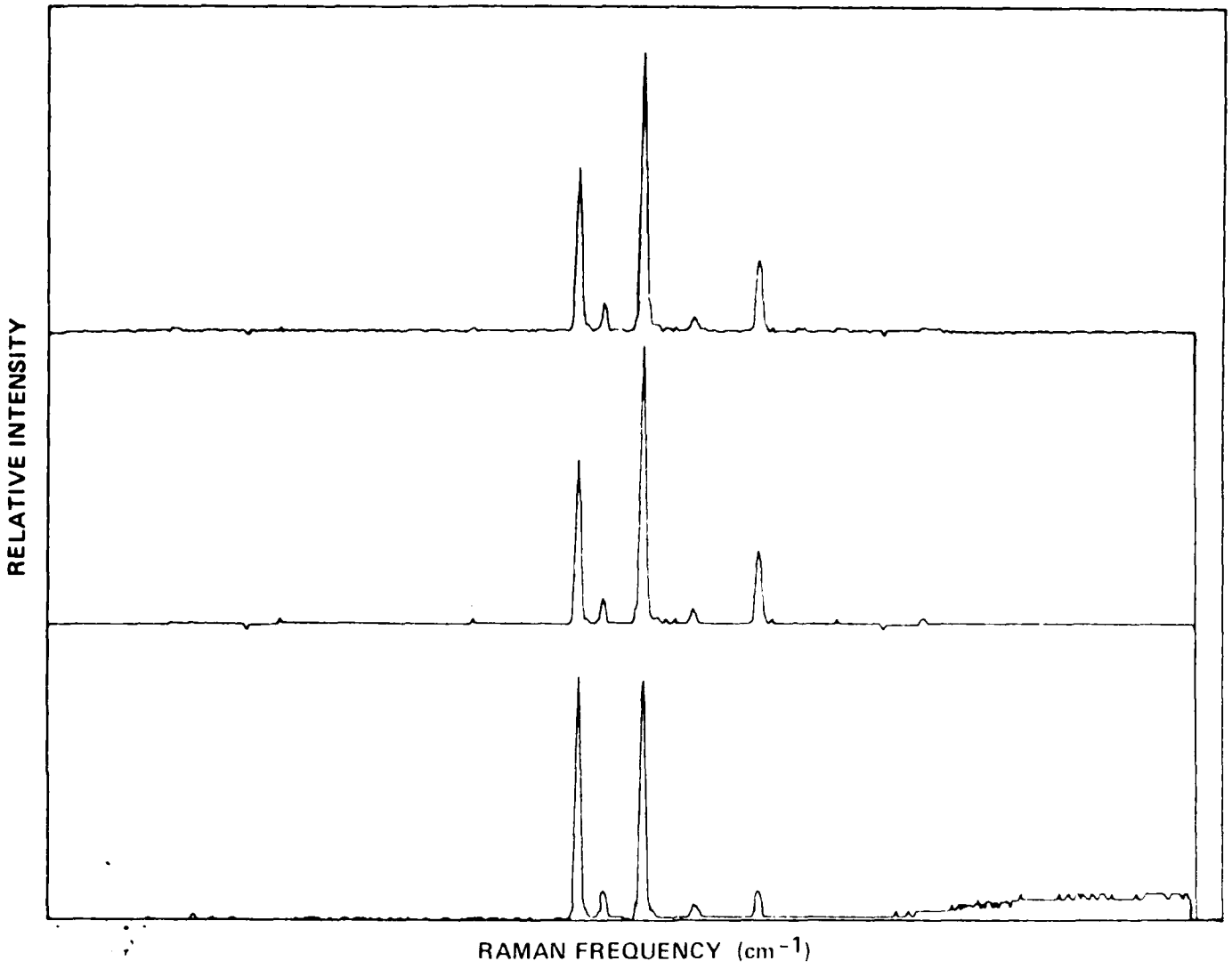

Figure 7. Time resolved (10-shot average) CARS spectra of the H$_2$ Q branch taken at nominal 6-sec intervals after ignition and shown sequentially from bottom to top

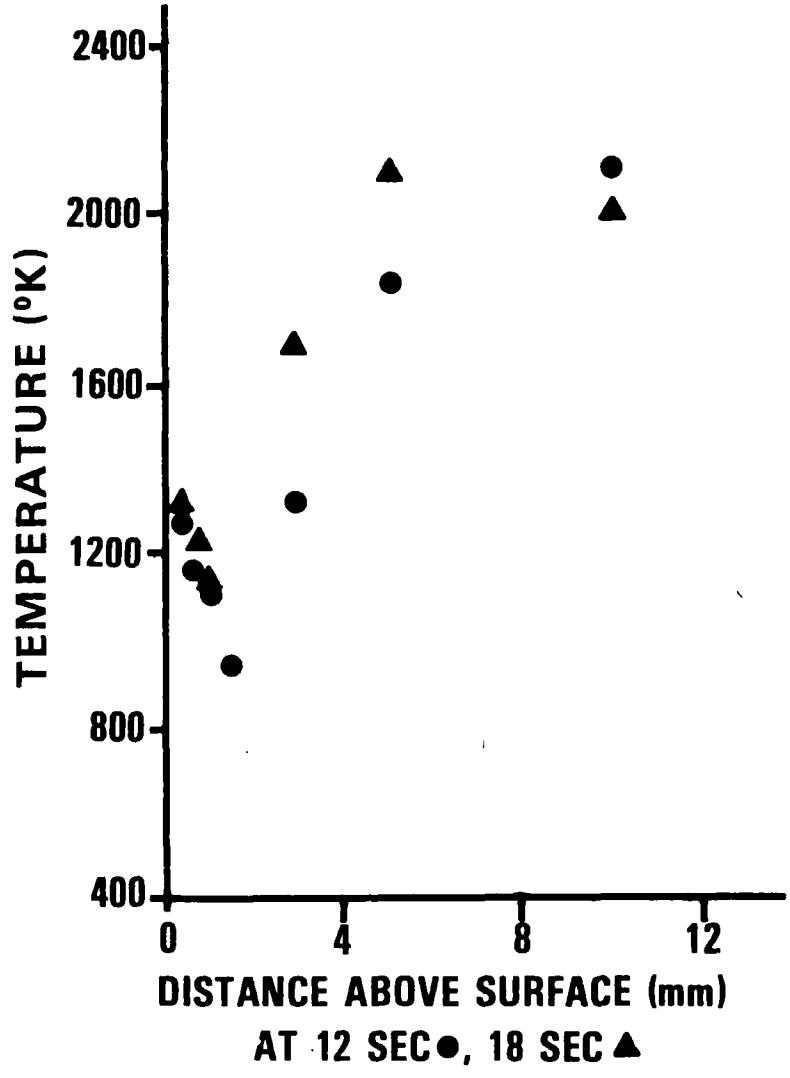

Figure 8. Temperature versus distance above surface at 12 and 18 seconds after nitramine composite ignition

REFERENCES

1 Norrish, R. G. W. and Porter, G., Nature (London) 164, 658 (1949).

2 Harris, L. E., Chemical Physics Letter, 93, 335 (1982).

3 Harris, L.E., Combustion and Flame, 53, 103 (1983).

4 Hall, R. J. and Eckbreth, A. C., Laser Applications, J. F. Ready and R. K. Erf (editors), 5, 213 (1984).

5 Bozlee, B. J. and Nibler, J. W., Journal of Chemical Physics, 84, 3798 (1986).

6 Holt, P. L., McCurdy, K. E., Adams, J. S., Burton, K. A., Weisman, R. B. and Engel, P. S., Journal of American Chemical Society, 107, 2180 (1985).

7 Aron, K. and Harris, L. E., Chemical Physics Letter, 103, 413 (1984).

8 Harris, L. E., Chemical Physics Letter, 109, 112 (1984).

9 Harris, L. E., Proceedings of the Tenth International Colloquium on Dynamics of Explosives and Reactive Systems, Berkely, CA (in press).

10 Haw, T., Cheung, W. Y., Chiu, G. C., and Harris, L. E., "A Study of Flame Species Using CARS," 40th Symposium on Molecular Spectroscopy, Ohio State University Abstract WH10, p 106 (1985).

11 Fendell, J., Harris, L. E., and Aron, K., "Theoretical Calculation of H_2 CARS Spectra for Propellant Flames," Technical Report ARLCD-TR-83048, ARDC, Dover, NJ (1983).

12 Dabrowski, I., Canadian Journal Physics, 62, 1639 (1984).

13 Greenhalgh, D. A. and Hall, R. J., Optical Communications, 57, 125 (1986).

14 Balakhnine, V. P., Vandooren, J., and van Tiggelen, P. J., Combustion and Flame, 28, 165 (1977).

15 Tabayaski, K. and Bauer, S. H., Combustion and Flame, 31 63 (1979).

16 Westbrook, C. K. and Dryer, D. L., Progress in Energy and Combustion Science, p 1 (1984).

17 Zabielski, M. P., "Mechanism and Reaction Dynamics Related to Methane Combustion", Report No. 956114-25, United Technology Research Center, East Hartford, CT (1984).

18 Miller, J. A., Branch, M. C., Mclean, W. J., Chandler, D. W., Mitchel, D. S., and Kee, R. J., "The Conversion of HCN to NC in H_2-O_2-HCN-AR Flames at Low Pressure," Report WSS/CT 84-36, Sandia National Laboratories, Livermore, CA (1984)

DISTRIBUTION LIST

Commander
Armament Research, Development
and Engineering Center
U.S. Army Armament, Munitions
and Chemical Command
ATTN: SMCAR-MSI (5)
SMCAR-TD, H. Krosser
SMCAR-TDC, H. Grundler
SMCAR-TDA, S. Hirschman
SMCAR-TDS, V. Lindner
SMCAR-TDD, J. Leccacorvi
SMCAR-AE, R. Bushey
P. Picard
SMCAR-AEE, J. Lannon
SMCAR-AEE-WE, F. Gilbert
SMCAR-AEE-WW, S. Bulusu
C. Capellos
F. Owens
SMCAR-AEP, D. Downs
SMCAR-AEP-R, L. Harris (10)
A. Beardell
B. Brodman
Y. Carignon
L. Stiefel
T. Vladimiroff
SMCAR-AER-T, P. Marinkas
Picatinny Arsenal, NJ 07806-5000

Commander
U.S. Army Armament, Munitions
and Chemical Command
ATTN: AMSMC-GCL(D)
AMSMC-QAH-T, J. Moskowitz
J. M. Argento
Picatinny Arsenal, NJ 07806-5000

Administrator
Defense Technical Information Center
ATTN: Accessions Division (12)
Cameron Station
Alexandria, VA 22304-6145

Director
U.S. Army Materiel Systems
Analysis Activity
ATTN: AMXSY-MP
Aberdeen Proving Ground, MD 21005-5066

Commander
Chemical Research, Development
and Engineering Center
U.S. Army Armament, Munitions
and Chemical Command
ATTN: SMCCR-MSI
Aberdeen Proving Grouond, MD 21010-5423

Commander
Chemical Research, Development
and Engineering Center
U.S. Army Armament, Munitions
and Chemical Command
ATTN: SMCCR-RSP-A
Aberdeen Proving Ground, MD 21010-5423

Director
Ballistic Research Laboratory
ATTN: AMXBR-OD-ST
SLCBR-IB, L. Watermier
A. Barrows
G. Adams
R. Fifer
M. Miller
T. Coffee
J. Heimeryl
C. Nelson
J. Vanderhoff
J. Anderson
Aberdeen Proving Ground, MD 21005-5066

Chief
Benet Weapons Laboratory, CCAC
Armament Research, Development and
Engineering Center
U.S. Army Armament, Munitions and
Chemical Command
ATTN: SMCAR-CCB-TL
Watervliet, NY 12189-5000

Commander
U.S. Army Armament, Munitions and
Chemical Command
ATTN: SMCAR-ESP-L
Rock Island, IL 61299-6000

Director
U.S. Army TRADOC Systems
Analysis Activity
ATTN: ATAA-SL
White Sands Missile Range, NM 88002

Director
Defense Advanced Research
Projects Agency
ATTN: LTC C. Buck
1400 Wilson Boulevard
Arlington, VA 22209

Commander
U.S. Army Materiel Command
ATTN: AMCDRA-ST
5001 Eisenhower Avenue
Alexandria, VA 22304

NASA
Langley Research Center
ATTN: MS 168, G. B. Northham
Hamption, VA 23365

Commander
U.S. Army Watervliet Arsenal
ATTN: SARWV-RD, R. Thierry
Watervliet, NY 12189

Director
U.S. Army Air Mobility Research
and Development Laboratory
Ames Research Center
Moffett Field, CA 94035

Commander
U.S. Army Electronics Research and
Development Command
ATTN: AMSEL-ED
DELSD-L
Fort Monmouth, NJ 07703-5301

Commander
U.S. Army Missile Command
ATTN: AMSMI-R
AMSMI-YDL
AMSMI-RK, D. J. Ifshin
W. Wharton
Redstone Arsenal, AL 35809-5252

Commander
U.S. Army Natick Research and
Development Command
ATTN: AMXRE, D. Sieling
Natick, MA 01762

Commander
U.S. Army Tank Automative Research
and Development Command
ATTN: AMSTA-TSL
Warren, MI 48090

Commander
U.S. Army White Sands
Missile Range
ATTN: STEWS-VT
White Sands Missile Range, NM 88002

Commander
U.S. Army Materials Technology
Laboratory
ATTN: AMXMR-ATL
Watertown, MA 02172

Commander
U.S. Army Research Office
ATTN: Technical Library
D. Squire
F. Schmiedeshaff
R. Ghirardelli
M. Ciftan
P.O. Box 12211
Research Triangle Park, NC 27706-2211

Office of Naval Research
ATTN: Code 473, G. Neece
Code 432, R. S. Miller
800 N. Quincy Street
Arlington, VA 22217

Commander
Naval Sea Systems Command
ATTN: W. Murrin, SEA-62R2
National Center
Bldg 2, Room 6E08
Washington, DC 20362

Commander
Naval Surface Weapons Center
ATTN: Library Branch, DX-21
G-23, J. L. East, Jr.
Dahlgren, VA 22448

Commander
Naval Surface Weapons Center
ATTN: Code 240, S. J. Jacobs
J. Sharma
Code 730
R-13, R. Bernecker
R-16, G. B. Wilmot
White Oak
Silver Spring, MD 20910

Commander
Naval Underwater Systems Center
Energy Conversion Department
ATTN: Code 5B331, R. S. Lazar
Newport, RI 02840

Commander
Naval Weapons Center
ATTN: Code 389, R. Derr
C. Thelen
Code 3891, T. Boggs
K. J. Graham
China Lake, CA 93555

Commander
Naval Research Laboratory
ATTN: Code 6180, L. Harvey
J. McDonald
E. Oran
J. Shnur
Code 6110, R. J. Doyle
Washington, DC 20375

Superintendent
Naval Postgraduate School
ATTN: Technical Library
Department of Aeronautics, D. Netzer
Monterey, CA 93940

Commander
Naval Ordnance Station
ATTN: Charles Dale
Technical Library
Indian Head, MD 20640-5000

Air Force Armament Laboratory
ATTN: AFATL-DLODL
Eglin Air Force Base, FL 32542-5000

AFOSR
ATTN: J. F. Masi
B. T. Wolfson
J. M. Tishkoff
D. Ball
L. Caveny
Bolling Air Force BAse
Washington, DC 20332

AFRPL (DRSC)
ATTN: D. George
R. Geisler
B. Goshgorian
W. Roe
D. Weaver
J. N. Levine
Edwards AFB, CA 93523-5000

National Bureau of Standards
U.S. Department of Commerce
ATTN: J. Hastie
T. Kashiwagi
H. Semerjian
M. Jacox
S. Ray
A. Carasso
K. Smyth
J. Stevenson
Washington, DC 20234

Lockheed Palo Alto Research
Laboratories
ATTN: Technical Information Center
Dept 52-35, George Lo
3521 Hanover Street
Palo Alto, CA 94304

Aerojet Solid Propulsion Co.
ATTN: P. Micheli
Sacramento, CA 96813

Atlantic Research Corporation
ATTN: M. K. King
5390 Cherokee Avenue
Alexandria, VA 22314

Atlantic Research Corporation
ATTN: R. H. W. Waesche
7511 Wellington Road
Gainsville, VA 22065

AVCO Corporation
AVCO Everett Research Laboratory
Division
ATTN: D. Stickler
2385 Revere Beach Parkway
Everett, MA 02149

Calspan Corporation
ATTN: E. B. Fisher
A.P. Trippe
P.O. Box 400
Buffalo, NY 14221

General Electric Armament
and Electrical Systems
ATTN: M. J. Bulman
Lakeside Avenue
Burlington, VT 05401

General Electric Company
Flight Propulsion Division
ATTN: Technical Library
Cincinnati, OH 45215

Hercules Powder Company
Alleghany Ballistic Lab
ATTN: R. Miller
Technical Library
Cumberland, MD 21501

Hercules, Incorporated
Bacchus Works
ATTN: B. Isom
K. P. McCarty
P.O. Box 98
Magna, UT 84044

IITRI
ATTN: M. J. Klein
10 West 35th Street
Chicago, IL 60615

Olin Corporation
Badger Army Ammunition Plant
ATTN: J. Ramnarace
Baraboo, WI 53913

Applied Combustion Technology, Inc.
ATTN: A. M. Varney
P.O. Box 17885
Orlando, FL 32860

Olin Corporation
New Haven Plant
ATTN: R. L. Cook
D. W. Riefler
275 Winchester Avenue
New Haven, CT 06504

Paul Gough Associates, Inc.
ATTN: P. S. Gough
P.O. Box 1614
Portsmouth, NH 03801

Physics International Company
2700 Merced Street
Leandro, CA 94577

Rockwell International Corp.
Rocketdyne Division
ATTN: C. Obert
J. E. Flanagan
A. Axeworthy
6633 Canoga Avenue
Canoga Park, CA 91304

Rockwell International Corp.
Rocketdyne Division
ATTN: W. Haymes
Technical Library
McGregor, TX 76657

Science Application, Inc.
ATTN: R. B. Edelman
23146 Cumorah Crest
Woodland Hills, CA 91364

Thiokol Corporation
Elkton Division
ATTN: E. Sutton
W. N. Brundige
Elkton, MD 21921

Thiokol Corporation
Huntsville Division
ATTN: D. Flanigan
R. Glick
Technical Library
Huntsville, AL 35807

Thiokol Corporation
Wasatch Division
ATTN: J. Peterson
Technical Library
P.O. Box 524
Brigham City, UT 84302

BDM Corporation
ATTN: T. P. Goddard
2600 Cearden Road
North Building
Monterey, CA 93940

TRW Systems Group
ATTN: H. Korman
One Space Park
Redondo Beach, CA 90278

United Technologies
Chemical Systems Division
ATTN: R. Brown
Technical Library
P.O. Box 358
Sunnyvale, CA 94086

Battelle Memorial Insitute
ATTN: Technical Library
R. Bartlett
505 King Avenue
Columbus, OH 43201

Brigham Young University
Department of Chemical Engineering
ATTN: M. W. Beckstead
Provo, UT 84601

California Insitute of Technology
204 Karmar Lab
Mail Stop 301-46
ATTN: F. E. C. Culick
1201 E. California Street
Pasadena, CA 91125

Georgia Institute of Technology
School of Aerospace Engineering
ATTN: B. T. Zinn
E. Price
W. C. Strahle
Atlanta, GA 30332

Institute of Gas Technology
ATTN: D. Gidaspow
3424 S. State Street
Chicago, IL 60616

Johns Hopkins University/APL
Chemical Propulsion Information Agency
ATTN: T. Christian
Johns Hopkins Road
Laurel, MD 20810

Massachusetts Institute of Technology
Department of Mechanical Engineering
ATTN: T. Toong
Cambridge, MA 02139

Massachusetts Institute of Technology
Laboratory for Information and
Decision Systems
ATTN: A. S. Willsky
Cambridge, MA 02139

Pennsylvania State University
Applied Research Laboratory
ATTN: G. M. Faeth
P.O. Box 30
State College, PA 16801

Pennsylvania State University
Department of Mechanical Engineering
ATTN: K. Kuo
University Park, PA 16801

Pennsylvania State University
Department of Material Sciences
ATTN: H. Palmer
University Park, PA 16801

Princeton Combustion Research Laboratories
ATTN: M. Summerfield
N. Messina
475 U.S. Highway One North
Monmouth Junction, NJ 08852

Princeton University
Forrestal Campus
ATTN: I. Glassman
K. Brezinsky
F. Dryer
Technical Library
P.O. Box 710
Princeton, NJ 08540

Princeton University
MAE Department
ATTN: F. A. Williams
Princeton, NJ 08544

Polytechnic Institute of NY
ATTN: S. Lederman
Route 110
Farmingdale, NY 11735

Purdue University
School of Mechanical Engineering
ATTN: J. Osborn
S. N. B. Murthy
N. M. Laurendeau
TSPC Chaffee Hall
West Lafayette, IN 47906

Purdue University
School of Aeronautics and Astronautics
ATTN: R. Glick
J. R. Osborn
West Lafayette, IN 47906

Rutgers State University
Department of Mechanical and Aerospace Engineering
ATTN: S. Temkin
University Heights Campus
New Brunswick, NJ 08903

SRI International
ATTN: Technical Library
D. Crosley
J. Barker
D. Golden
G. Smith
333 Ravenswood Avenue
Menlo Park, CA 94025

Stevens Institute of Technology
Department of Chemistry
and Chemical Engineering
ATTN: W. C. Ermler
Hoboken, NJ 07030

Stevens Institute of Technology
Dvidson Laboratory
ATTN: R. McAlevy
Hoboken, NJ 07030

United Technology
ATTN: Alan Ecbreth
Robert Hall
Research Center
East Hartford, CT 06108

General Motors Corporation
ATTN: J. H. Bechtel
R. Teets
Warren, Michigan 48090

System Research Laboratory
ATTN: L. Goss
2600 Indian Ripple Rd
Dayton, OH 45440

University of California
Lawrence Livermore National Laboratory
ATTN: Library
A. C. Buckingham
Livermore, CA 94550

Exxon Research and Engineering Company
ATTN: A. Dean
M. Chou
P.O. Box 8
Linden, NJ 07036

Ford Motor Company
Research Staff
ATTN: K. Marko
L. Rimai
Dearborn, Michigan 48120

Sandia National Laboratories
Combustion Sciences Department
ATTN: R. Cattolica
D. Stephenson
P. Mattern
Livermore, CA 94550

Sandia National Laboratories
ATTN: M. Smoke
Division 8353
Livermore, CA 94550

Rensselaer Polytechnic Institute
Dept. of Chem. Engineering
ATTN: A. Fontijn
Troy, NY 12181

University of California, San Diego
Energy Center and Department
of Applied Mechanics
ATTN: S. S. Penner
La Joll, CA 92037

University of California
Dept. of Mechanical Engr
ATTN: J. W. Daily
Berkeley, CA 94720

University of Dayton Research Institute
ATTN: D. Campbell
Dayton, OH 45406

University of Florida
Dept. of Chemistry
ATTN: J. Winefordner
Gainesville, FL 32601

University of Illinois
Dept. of Mechanical Engr
ATTN: H. Krier
S. L. Soo
144 MEB, 1206 W. Green St.
Urbana, IL 61801

University of Minnesota
Dept. of Mechanical Engr
ATTN: E. Fletcher
Minneapolis, MN 55455

University of California,
Santa Barbara
Quantum Institute
ATTN: K. Schofield
M. Steinberg
Santa Barbara, CA 93106

University of Southern California
Department of Chemistry
ATTN: S. Benson
Los Angeles, CA 90007

Standford University
Department of Mech Engr
ATTN: R. Hanson
Sandford, CA 93106

Standford University
Department of Physics
ATTN: A. Macovski
Palo Alto, CA 94305

University of Texas
Department of Chemistry
ATTN: W. Gardiner
H. Schaefer
Austin, TX 78712

University of Utah
Dept. of Chemical Engineering
ATTN: A. Baer
G. Flandro
Salt Lake City, UT 84112